An analytical model for mechanical etching of glass by powder blasting

J.H.M. ten Thije Boonkkamp and J.K.M. Jansen
Department of Mathematics and Computer Science, Eindhoven University of Technology,
PO Box 513, 5600MB Eindhoven, The Netherlands

Abstract. A nonlinear hyperbolic partial differential equation modelling the etching of glass by powder blasting is proposed. This equation is solved by means of the characteristic strip equations. The analytical solution is in reasonable agreement with measurements.
AMS Subject Classification: 35F25, 35L60, 33C05.
Keywords: Powder blasting; nonlinear hyperbolic equation; characteristic strip equations; shocks.

1 Introduction

The increase in size of modern television screens has driven a trend towards lightweight, shallow displays to replace the current heavy, bulky cathode ray tube type of displays. Several basic principles for display design have been studied or are still being researched; for an overview see e.g. [17]. Some of these display principles require a vacuum enclosure for their operation; see e.g. [6]. In order to make lightweight displays, internal structures are required to support the vacuum envelope. Since these structures must not get in the way of the display function, they must be very accurately positioned. Furthermore, they should consist of dielectric material that has the same thermal expansion coefficient as the transparent, vacuum proof front panel. Therefore, only structures of inorganic glass or ceramics are appropriate. In [6] a display is studied, which makes use of thin, patterned glass plates as supporting structure, where electrons can travel through holes or trenches in the glass plates. These glass plates thus have to be very accurately patterned with holes or trenches over large surfaces (up to $1m^2$).

The high accuracy patterning of glass plates at low cost is still an ongoing challenge. A promising technique studied here for this purpose is the mechanical etching by solid particle erosion, more commonly named powder- or sandblasting [10]. Patterned etching by sandblasting has been used mainly for the decoration of glass and mirrors, where the scattering of light at eroded parts of the surface contrasts attractively with the smooth unaffected parts of the surface. Although the decorative application has been used for many years, it did not need fundamental understanding. Furthermore, the erosion mechanism at the basis of the process, namely solid particle impact, has been studied scientifically as the undesirable phenomenon damaging aircraft and rocket parts. Since this effort was primarily directed towards preventing erosion, little was known about the implications of using solid particle erosion as a high-accuracy industrial etching process.

The physics of solid particle erosion is presented in [13]. In particular, the erosion rate of an uncovered glass plate blasted with an abrasive powder is studied. Conversely, in this paper we investigate the formation of patterns by erosion of surfaces that are locally protected with an erosion resistant mask. We present a first model for the evolution of a substrate surface under the continuous impacts of particles. The problem posed has some similarities with the erosion of structures at far finer scales, using ion sputtering; see e.g. [4, 19, 8]. In this field models have been derived to describe the evolution of surfaces in 2D and 3D. The characteristics of the solid-particle erosion process, however, differ in a number of ways from that of ion sputtering, posing specific problems and making the ion sputtering experience of limited use for the powder blasting process.

We have organized our paper as follows. In Section 2 we give a brief outline of the physics of powder erosion. In particular, we propose a model for the erosion rate E, based on measured data. Subsequently, in Section 3, we present a mathematical model for the erosion of glass, which consists of a hyperbolic partial differential equation for the surface position z or its slope p. In Section 4 we formulate the corresponding characteristic strip equations, which are subsequently solved in Section 5.

2 Physics of powder erosion

In powder erosion of brittle materials, sharp and abrasive particles in the powder cause deformations and micro-cracks in the target material. The formation of micro-cracks is governed by the kinetic energy of the erosive particles [13]. Chipping of target material above the cracks is the dominant erosion mechanism. The rate at which substrate material is removed is determined by the erosion rate E, which is defined as the ratio of the mass loss of the substrate and the mass of the erodent used.

There are several models for the erosion rate [13, 3, 11, 7]. In all these models, the erosion rate depends on the particle impact velocity $\mathbf{v}$. At normal impact, the erosion rate is proportional to a power of the magnitude of the impact velocity, i.e.

$$E = C\,|\mathbf{v}|^k, \tag{1}$$

where $C > 0$ is an empirical constant. Also the exponent k is determined experimentally, and its value varies between 2 and 4 [5]. On the other hand, theoretical models predict the value $k = 7/3$; see e.g. [13, 3].

At oblique impact the erosion rate decreases. In this case, the erosion rate is roughly proportional to the component of the impact velocity normal to the substrate [2, 16, 12, 20]. This can be observed from Figure 1, which shows the erosion rate of glass exposed to alumina particles, as a function of the normal component of the impact velocity; see also [14, 15]. Therefore, we adopt the following model:

$$E = C\big(\,|\mathbf{v}|\,\cos\vartheta\big)^k, \tag{2}$$

where ϑ is the angle between the impact velocity vector $\mathbf{v}$ and the inward normal $\mathbf{n}$ to the surface. Note that for $\vartheta = 75^\circ$, i.e. at glancing contact, the factor C in (2) is somewhat different from the value at smaller angles ϑ.

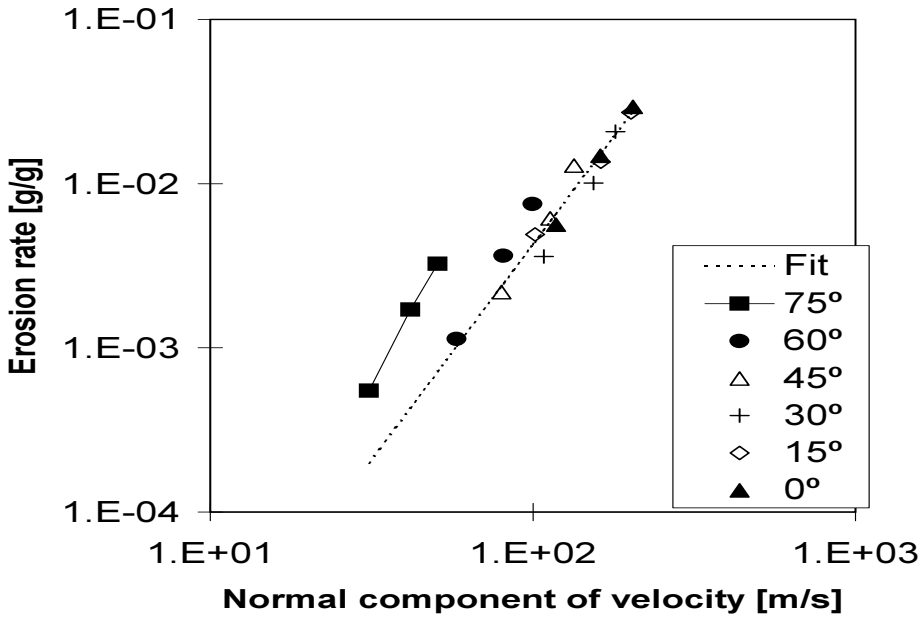

Figure 1: The erosion rate of glass as a function of the normal component of the impact velocity. The figures in the box give the angle between the impact velocity and the inward normal to the surface.
(courtesy P.J. Slikkerveer, Philips Research Laboratories, Eindhoven)

Figure 2 shows the formation of a pattern in a glass plate by masked erosion. The mask considered has a circular hole and is exposed to a constant particle mass flux, i.e. the particle flux and the impact velocity are constant. The photographs have been made by time-lapse photography, exposing a picture at fixed time intervals. Some characteristics of the erosion process can be seen from these photographs. First, the hole is shallow close to the edge of the mask and has a sharp tip in the middle. The reason for this is, that due to the finite particle size, not all particles contribute to the erosion process close to the mask. On the other hand, for a wide, shallow hole we would get a flat bottom in the centre. Secondly, with increasing depth the rate of growth of the hole decreases. This can be explained by the dependence of the erosion rate on the angle of impact ϑ. Finally, with increasing depth the hole takes an udder shape. This is probably caused by rebounding particles from the steep slopes at the sides of the pattern [14]. These particles are focussed to the centre of the pattern, where they generate additional erosion. We will not consider this so-called second-strike effect in this paper.

3 Mathematical model for powder erosion

In this section we introduce a mathematical model for the displacement of a surface due to erosion by abrasive particles. Subsequently, we consider two special cases, viz. a one-dimensional trench and a rotationally symmetric hole.

Consider an initially flat substrate of brittle material, covered with a mask. In Figure 3 we introduce

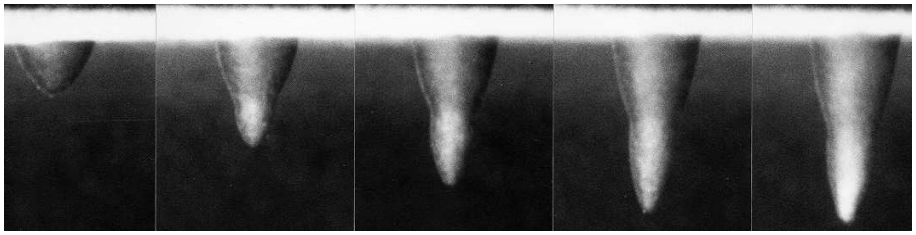

Figure 2: Pattern formation in glass by masked erosion. (courtesy P.J. Slikkerveer, Philips Research Laboratories, Eindhoven)

an (x, y, z)-coordinate system, where the (x, y)-plane coincides with the initial substrate and where the positive z-axis is directed into the material. A flux of particles with velocity $\mathbf{v}$ in the positive z-direction hits the substrate and removes material. The position of the surface at time t is described by the function $z = z(x, y, t)$. We now derive a kinematic condition for the surface. Let R denote the velocity of the surface in the direction of the unit normal $\mathbf{n}$ on the surface, which is directed into the material and is given by

$$\mathbf{n} = \frac{1}{\sqrt{1 + z_x^2 + z_y^2}} \begin{pmatrix} -z_x \\ -z_y \\ 1 \end{pmatrix}. \tag{3}$$

Consider a point $P(x_0, y_0, z_0)$ on the surface at time t_0. During a small time interval δt this point is displaced over a distance $R\,\delta t$ in the direction of $\mathbf{n}$ to the point $P'(x_0 + \delta x, y_0 + \delta y, z_0 + \delta z)$. It is clear that the dispacements δx, δy and δz are given by

$$\begin{aligned} \delta x &= R\delta t \mathbf{n}\cdot\mathbf{e}_x = -\frac{R\delta t z_x}{\sqrt{1 + z_x^2 + z_y^2}}, \\ \delta y &= R\delta t \mathbf{n}\cdot\mathbf{e}_y = -\frac{R\delta t z_y}{\sqrt{1 + z_x^2 + z_y^2}}, \\ \delta z &= R\delta t \mathbf{n}\cdot\mathbf{e}_z = \frac{R\delta t}{\sqrt{1 + z_x^2 + z_y^2}}. \end{aligned} \tag{4}$$

On the other hand, we have

$$\begin{aligned} \delta z &= z(x_0 + \delta x, y_0 + \delta y, t_0 + \delta t) - z(x_0, y_0, t_0) \\ &= z_x(x_0, y_0, t_0)\delta x + z_y(x_0, y_0, t_0)\delta y + z_t(x_0, y_0, t_0)\delta t + \mathcal{O}(\delta t^2). \end{aligned} \tag{5}$$

Combining formulae (4) and (5) and taking the limit $\delta t \to 0$, we obtain the following equation for z:

$$z_t - R\sqrt{1 + z_x^2 + z_y^2} = 0. \tag{6}$$

Initial and boundary conditions for (6) will be specified later.

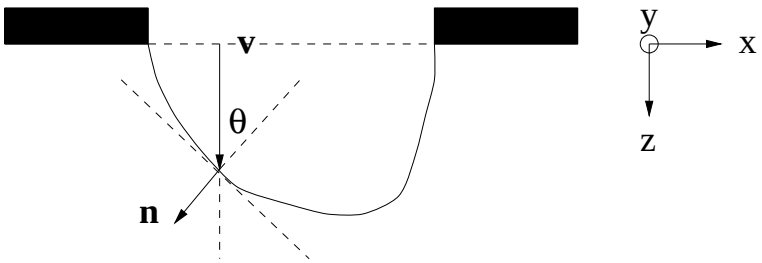

Figure 3: Cross section of a two-dimensional hole in the substrate.

For R we adopt the model [14]

$$R = \frac{1}{\rho} E\, \mathbf{\Phi}\cdot\mathbf{n} = \frac{1}{\rho} E\, \Phi \cos\vartheta, \tag{7}$$

where ρ is the mass density of the material, E the erosion rate, $\mathbf{\Phi} = \Phi \mathbf{e}_z$ the particle mass flux in the direction of $\mathbf{v}$ and ϑ the angle between $\mathbf{v}$ and $\mathbf{n}$. This means that only the particle flux perpendicular to the surface contributes to the velocity R of the surface. Likewise, the erosion rate E only depends on the normal component $\mathbf{v}\cdot\mathbf{n}$ of the particle velocity $\mathbf{v} = v\mathbf{e}_z$, and is given by (2). The particle mass flux $\Phi(x, y)$ will be specified later. Substitution of (7) and (2) into (6) gives

$$z_t - \frac{C}{\rho} v^k \Phi \left(1 + z_x^2 + z_y^2\right)^{-k/2} = 0, \tag{8}$$

where we have used that $\cos\vartheta = 1/\sqrt{1 + z_x^2 + z_y^2}$.

Next, we make equation (8) dimensionless. Introducing a characteristic length scale L, a characteristic particle mass flux $\tilde{\Phi}$ and the characteristic time $T = L\rho/(C\tilde{\Phi}v^k)$, we obtain in a straightforward way

$$z_t - \Phi(x, y)\left(1 + z_x^2 + z_y^2\right)^{-k/2} = 0. \tag{9}$$

The characteristic length L can be the width of a one-dimensional trench or the radius of a rotationally symmetric hole. Note that T is the time needed to propagate the surface over a distance L, when the particles hit the surface perpendicularly with mass flux $\tilde{\Phi}$.

The first special case we consider is the growth of a one-dimensional trench. Let x denote the transverse coordinate in the trench as indicated in Figure 3, then equation (9) reduces to

$$z_t + \Phi(x)\, f(z_x) = 0, \quad 0 < x < 1, t > 0, \tag{10}$$

where the function $f = f(p)$ is defined by

$$f(p) = -\left(1 + p^2\right)^{-k/2}. \tag{11}$$

Equation (10) is supplemented with the following initial and boundary conditions:

$$z(x, 0) = z_0(x), \quad 0 < x < 1, \tag{12}$$

$$z(0,t) = z(1,t) = 0, \quad t > 0. \tag{13}$$

For the initial profile $z_0(x)$ we usually take $z_0(x) = 0$; however other choices are also possible. The boundary conditions in (13) mean that the trench cannot grow at the ends $x = 0$ and $x = 1$.

An alternative formulation of the formation of a trench is in terms of the slope $p = z_x$. If we differentiate equation (10) and initial condition (12) with respect to x, we obtain the following initial value problem for p:

$$p_t + \big(\Phi(x)\, f(p)\big)_x = 0, \quad 0 < x < 1, t > 0, \tag{14}$$

$$p(x,0) = z_0'(x), \quad 0 < x < 1. \tag{15}$$

Note that we do not have boundary conditions for p, however, we do not need them either as will become apparent in Section 4.

The second special case concerns the growth of a rotationally symmetric hole. Assume that the hole in the substrate has a circular shape. It is convenient to express equation (9) in polar coordinates (r, ϕ), where the origin is located at the centre of the hole. Assuming rotational symmetry, equation (9) can be written as

$$z_t + \Phi(r)\, f(z_r) = 0, \quad 0 < r < 1, t > 0. \tag{16}$$

Note that the particle mass flux now depends on r. Suitable initial and boundary conditions are

$$z(r,0) = z_0(r), \quad 0 < r < 1, \tag{17}$$

$$z(1,t) = 0, \quad t > 0. \tag{18}$$

In this case we have only one boundary condition at $r = 1$, stating that the hole does not grow at the edge.

Comparing the initial boundary value problems (10)-(13) and (16)-(18), it is clear that the profiles $z = z(x,t)$ for a one-dimensional trench and $z = z(r,t)$ for a cylindrically symmetric hole are alike. In the following, we only consider the one-dimensional trench problem.

4 Characteristic strip equations

In this section we present the characteristic strip equations of the initial value problems (10)-(12) and (14)-(15). We assume that we have an initially flat substrate. Furthermore, we specify the particle mass flux Φ.

Consider the following partial differential equations for the surface position $z(x,t)$ and its slope $p(x,t) = z_x(x,t)$:

$$z_t - \Phi(x)\big(1 + z_x^2\big)^{-k/2} = 0, \tag{19}$$

$$p_t - \big(\Phi(x)\big(1 + p^2\big)^{-k/2}\big)_x = 0, \quad 0 < x < 1, t > 0,$$

together with the initial conditions

$$z(x,0) = p(x,0) = 0, \quad 0 < x < 1. \tag{20}$$

Introducing the variable $q = z_t$, the first partial differential equation in (19) can be written in the canonical form

$$F(x,t,z,p,q) := q - \Phi(x)\big(1+p^2\big)^{-k/2} = 0. \tag{21}$$

The solution of the Cauchy problem for z, given by (21) and the corresponding initial condition in (20), can be constructed by solving the following initial value problem [9]:

$$\begin{aligned}
&\tfrac{\mathrm{d}x}{\mathrm{d}s} = F_p = \Phi(x)\tfrac{kp}{(1+p^2)^{k/2+1}}, && x(0;\tau) = \tau,\\
&\tfrac{\mathrm{d}t}{\mathrm{d}s} = F_q = 1, && t(0;\tau) = 0,\\
&\tfrac{\mathrm{d}z}{\mathrm{d}s} = pF_p + qF_q = \Phi(x)\tfrac{1+(k+1)p^2}{(1+p^2)^{k/2+1}}, && z(0;\tau) = 0,\\
&\tfrac{\mathrm{d}p}{\mathrm{d}s} = -(F_x + pF_z) = \Phi'(x)\tfrac{1}{(1+p^2)^{k/2}}, && p(0;\tau) = 0,\\
&\tfrac{\mathrm{d}q}{\mathrm{d}s} = -(F_t + qF_z) = 0, && q(0;\tau) = \Phi(\tau),
\end{aligned} \tag{22}$$

where s and τ are the parameters along the characteristics and the initial curve, respectively. The equations in (22) are referred to as the characteristic strip equations. The initial condition for q follows from the partial differential equation (21) and the initial conditions for the other variables. At the same time, the first, second and fourth differential equations plus corresponding initial values determine the characteristics of the Cauchy problem for p, given by the second partial differential equation in (19) and the corresponding initial condition in (20). Note that the solution of the second and fifth equations is trivial, and we find

$$\begin{aligned}
&t(s;\tau) = s,\\
&q(s;\tau) = \Phi(\tau).
\end{aligned} \tag{23}$$

The formal solution procedure for the other equations is as follows. We solve the first, third and fourth equations and find $x = x(t;\tau)$, $z = z(t;\tau)$ and $p = p(t;\tau)$. Inverting the first function gives $\tau = \tau(x,t)$ and substitution of the latter expresssion gives the final solution $z(x,t) := z(t;\tau(x,t))$ and $p(x,t) := p(t;\tau(x,t))$. In the following we use the notation $v(t;\tau)$ or $v(x;\tau)$ for a generic variable v, to indicate that an expression only holds along a characteristic parametrized by t or x. The parameter τ denotes that the characteristic passes through the point $(\tau,0)$. On the other hand, we use the notation $v(x,t)$ if an expression holds in a part of the (x,t)-plane.

A first obvious choice for the dimensionless particle mass flux would be $\Phi(x) = 1$. The solution of the initial value problem (22) in this case is trivial, and we find $z(x,t) = t$ and $p(x,t) = 0$, corresponding with a flat bottom hole. This particular solution is in contrast with experimental results, which show slanted sides near the edges of the mask; see Figure 2. As observed in Section 2, this is due to the finite

particle size of the eroding powder. In order to take into account the finite particle size, we choose the following particle mass flux:

$$\Phi(x) = \begin{cases} x/\delta & \text{if} \quad 0 \le x < \delta, \\ 1 & \text{if} \quad \delta \le x \le 1-\delta, \\ (1-x)/\delta & \text{if} \quad 1-\delta < x \le 1, \end{cases} \tag{24}$$

where $0 < \delta \ll 1$. The parameter δ is characteristic of the particle size of the eroding powder. As a consequence of (24), the growth rate of the surface position close to the mask is smaller than in the middle of the hole. Since $\Phi(0) = \Phi(1) = 0$, we obtain from (22) the solutions $x(t;0) = z(t;0) = 0$ and $x(t;1) = 1$, $z(t;1) = 0$, implying that the boundary conditions (13) for z are automatically satisfied. Moreover, since $\Phi'(0) = 1/\delta$, we can directly compute $p(t;0)$ from the fourth equation in (22); likewise we can compute $p(t;1)$. Consequently, we may not give boundary conditions for p.

Note that, since $\Phi'(x)$ is discontinuous at the edges $x = \delta$ and $x = 1-\delta$ of the interior domain where $\Phi(x) = 1$, the solution of the partial differential equation for p in (19) can only be a weak solution [9] and it is anticipated that shocks will emerge from these edges. Let $x = \xi_{s,1}(t)$ and $x = \xi_{s,2}(t)$ denote the location of the shocks at time t originating at $x = \delta$ and $x = 1-\delta$, respectively. Each point $(\xi_{s,i}(t), t)$ $(i = 1, 2)$ on these shocks is connected to two different characteristics that exist on both sides of the shocks. The speed of these shocks is given by

$$\frac{\mathrm{d}\xi_{s,i}}{\mathrm{d}t}[p] = -[\Phi(x)(1+p^2)^{-k/2}], \ (i = 1, 2) \tag{25}$$

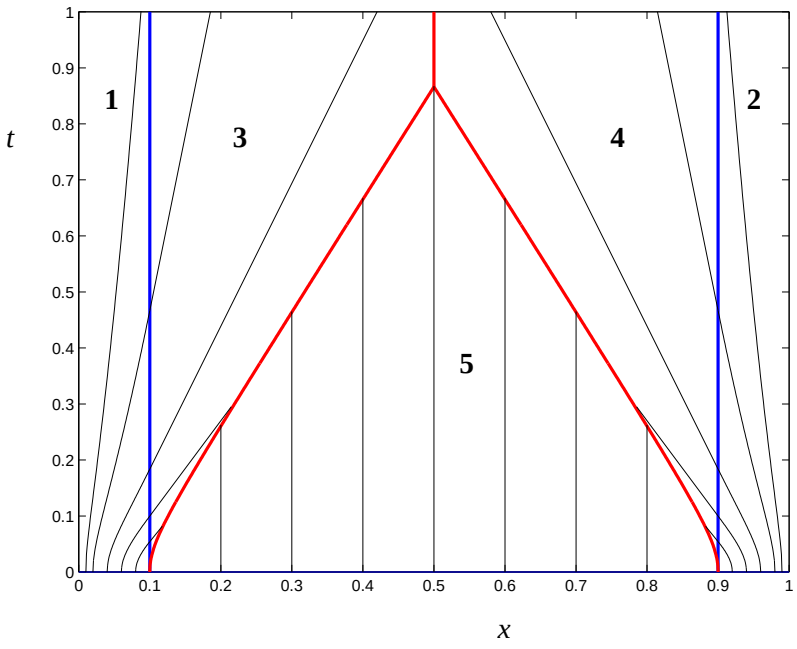

Figure 4: Characteristics and shocks of a one-dimensional trench, for $\delta = 0.1$ and $k = 2$.

where $[v]$ denotes the jump of the variable v across the shock. Thus, we can distinguish the following five regions in the (x,t)-plane: the left boundary layer $0 \le x \le \delta$ (region 1), the right boundary layer $1-\delta \le x \le 1$ (region 2), the interior domain left of the first shock (region 3), the interior domain right of the second shock (region 4) and the region between the two shocks (region 5); see Figure 4. Region 3 is the range of influence of the points in the left boundary layer, and likewise, region 4 is the range of influence of the points in the right boundary layer. In the following we will solve the system (22) in these five regions. Note, that the location of the shocks depends on the solution through the equations (25) and has to be computed as well.

5 Analytical solution method

The exact solution of the initial value problem (22) is computed in this section. The special case $k = 2$ is discussed in [18].

First, consider region 1. If we choose x as parameter along the characteristics instead of t, we can derive from (22) the following differential equations for the slope p and the surface position z,

$$\begin{aligned} \frac{\mathrm{d}p}{\mathrm{d}x} &= \frac{1}{x}\frac{1+p^2}{kp}, \\ \frac{\mathrm{d}z}{\mathrm{d}x} &= \frac{1+(k+1)p^2}{kp}. \end{aligned} \tag{26}$$

Taking into account the initial conditions $x(0;\tau) = \tau$ and $p(0;\tau) = 0$ in (22), we can solve the first equation and find

$$p(x;\tau) = \sqrt{\left(\frac{x}{\tau}\right)^{2/k} - 1}. \tag{27}$$

Combining both differential equations in (26), we find the following simple equation for z

$$\frac{\mathrm{d}z}{\mathrm{d}x} = p + \frac{1+p^2}{kp} = p + x\frac{\mathrm{d}p}{\mathrm{d}x}, \tag{28}$$

and together with the initial conditions $z(0;\tau) = p(0;\tau) = 0$ in (22) it has the solution

$$z(x;\tau) = xp(x;\tau). \tag{29}$$

The solutions in (27) and (29)) give p and z along the characteristic through the point $(\tau, 0)$ on the initial curve. The location of this characteristic follows from the differential equation

$$\frac{\mathrm{d}x}{\mathrm{d}t} = \frac{k\tau}{\delta}\frac{\sqrt{\left(x/\tau\right)^{2/k} - 1}}{\left(x/\tau\right)^{2/k}}, \tag{30}$$

which follows readily after substitution of (27) into the differential equation for x in (22). Integration of (30) subject to the initial condition $x(0;\tau) = \tau$ and choosing p as the independent variable gives the relation

$$\frac{t}{\delta} = \mathcal{T}(p) := \int_0^p \left(1 + r^2\right)^{k/2} \mathrm{d}r. \tag{31}$$

The integral in (31) can be expressed in terms of a hypergeometric function ${}_2F_1\big(a, b; c; z\big)$, resulting in the following alternative expression for t/δ [1]:

$$\frac{t}{\delta} = p\big(\,1 + p^2\,\big)^{k/2}\,{}_2F_1\big(\,-k/2, 1; 3/2; \sin^2\vartheta\,\big), \quad \sin\vartheta = \frac{p}{\sqrt{1+p^2}}, \tag{32}$$

where ϑ is the angle between the impact velocity $\mathbf{v}$ and the inward normal $\mathbf{n}$; see Figure 3. Alternatively, formulae (31) and (32) can be obtained by direct integration of the differential equation for p in (22). Points (x, t) on the characteristic through $(\tau, 0)$ are thus determined by (27) and (31). Note that the slope p in region 1 is a function of t/δ only and is independent of the space coordinate x. When computing the solution in region 1 at a given time level t, we first solve equation (31) for p and subsequently compute z from (29).

From (27), (29) and (31), we see that the characteristic through $(\tau, 0)$ $(0 < \tau < \delta)$ reaches the edge $x = \delta$ at time $t_1(\tau)$, with slope $p_1(\tau)$ and surface position $z_1(\tau)$ given by

$$\begin{aligned} p_1(\tau) &:= \sqrt{\left(\frac{\delta}{\tau}\right)^{2/k} - 1}, \\ z_1(\tau) &:= \delta p_1(\tau), \\ t_1(\tau) &:= \delta \mathcal{T}(p_1(\tau)), \end{aligned} \tag{33}$$

with $\mathcal{T}(p)$ defined in (31). These are the 'initial' conditions for the solution of initial value problem (22) in region 3.

Now, consider region 3. Since $\Phi'(x) = 0$ in region 3, the slope p is constant along characteristics and consequently, the differential equations in (22) can be easily solved. We find

$$\begin{aligned} p(x;\tau) &= p_1(\tau), \\ z(x;\tau) &= z_1(\tau) + \frac{1 + (k+1)p_1^2(\tau)}{k p_1(\tau)}(x - \delta), \\ t(x;\tau) &= t_1(\tau) + \frac{\left(\,1 + p_1^2(\tau)\,\right)^{k/2+1}}{k p_1(\tau)}(x - \delta), \end{aligned} \tag{34}$$

with $p_1(\tau)$, $z_1(\tau)$ and $t_1(\tau)$ defined in (33). The characteristics in this region are straight lines and are displayed in Figure 4. To compute the solution at a given point (x, t), we first have to solve the third equation in (34) for $p_1(\tau)$ and subsequently compute $p(x, t)$ and $z(x, t)$ from the other two equations.

The solution of (22) in region 5 is trivial, and is given by

$$\begin{aligned} x(t;\tau)&=\tau, \\ p(x,t)&=0, \\ z(x,t)&=t, \end{aligned} \tag{35}$$

see Figure 4. The characteristics are now vertical lines through $(\tau, 0)$, corresponding to a flat surface.

Since the particle mass flux (24) is symmetric around $x = 0.5$, it is also clear that the solution of the initial value problem (22) is symmetric around $x = 0.5$. Consequently, the solution in regions 2 and 4 can be easily obtained from the corresponding solutions in region 1 and 3, respectively. However, for the sake of brevity, we omit the explicit formulae.

Finally, we have to determine the location of the shocks. We only consider the first shock, emanating from the edge $x = \delta$. The computation of the second shock is completely analogous. The evolution of the first shock is determined by the jump condition (25), which in this case leads to the initial value problem

$$\frac{\mathrm{d}\xi_{s,1}}{\mathrm{d}t} = \frac{1}{p_{s,1}}\Big(1 - \big(1 + p_{s,1}^2 \big)^{-k/2} \Big), \quad \xi_{s,1}(0) = \delta, \tag{36}$$

with $p_{s,1} = p_1(\tau)$ the value of the slope just left of the shock, on the characteristic through $(\delta, t_1(\tau))$. Thus, the following relation holds between $p_{s,1}$ and $\xi_{s,1}$:

$$\frac{\xi_{s,1} - \delta}{t - t_1(\tau)} = \frac{k p_{s,1}}{\big(1 + p_{s,1}^2 \big)^{k/2+1}}. \tag{37}$$

Combining relation (37) with the formulae for $t_1(\tau)$ given in (33) and (31), differentiating the resulting equation with respect to t and substituting (36), we find the following initial value problem for $p_{s,1}$:

$$\frac{\mathrm{d}p_{s,1}}{\mathrm{d}t} = \frac{p_{s,1}^2}{\big(1 + p_{s,1}^2 \big)^{k/2}} \frac{\Big(k - \big(1 + p_{s,1}^2 \big) \frac{\left(1+p_{s,1}^2 \right)^{k/2} - 1}{p_{s,1}^2} \Big) / \big(1 - p_{s,1}^2 \big)}{\delta - \frac{(k+1)p_{s,1}^2 - 1}{p_{s,1}^2 - 1}\, \xi_{s,1}}, \quad p_{s,1}(0) = 0. \tag{38}$$

The initial value for $p_{s,1}$ follows from e.g. equation (31). Note that the right hand side of (38) is not defined for $t = 0$, and can only be computed using Taylor series for $\xi_{s,1}(t)$ and $p_{s,1}(t)$. The propagation of the shock is determined by the differential equations (36) and (38), which we have to solve numerically. The result is shown in Figure 4.

We have collected the results of this section in Figure 5, which gives the analytical solutions for z and p at time levels $t = 0.0, 0.1, \cdots, 1.0$ for $\delta = 0.1$ and $k = 2, 2.33, 3, 4$. Figure 5 nicely displays the features of the solution: a slanted surface in the boundary layers, a flat bottom in the interior domain and a curved surface in between. Also, the inwards propagating shocks are clearly visible. Moreover, for increasing k, the slopes decrease resulting in more shallow holes.

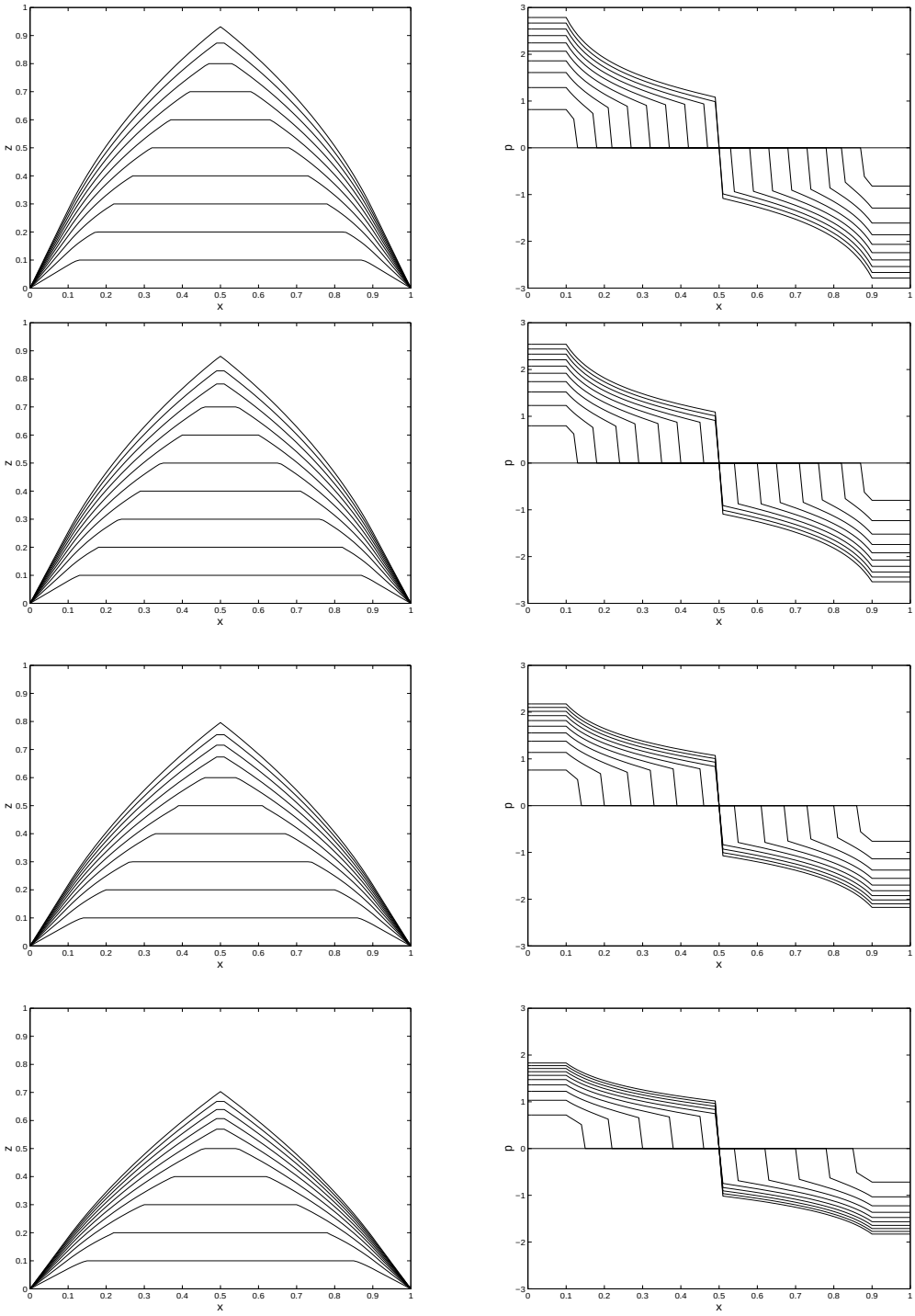

Figure 5: Analytical solution for the surface position (left) and its slope (right) of a one-dimensional trench. Parameter values are $\delta = 0.1$ and (from top to bottom) $k = 2, 2.33, 3$ and 4.

To validate our model, we compare in Figure 6 the analytical solution with experimental results at four different time levels, for the erosion of a trench. All surfaces are dimensionless according to the scaling in Section 3. We have computed the surfaces with $k = 7/3$ and $\delta = 0.1$. We see a reasonable qualitative agreement between analytical and experimental results. Both show the shallow, flat bottom solution in the middle of the hole at $t = 0.5$. However, the analytically computed hole at $t = 0.5$ is somewhat deeper than the experimental one. The reason for this is probably the shadow effect of the mask, which is not included in the analytical model. For $t \geq 1.6$, the experimental surfaces show an udder shape in the middle of the hole, which is caused by rebounding particles from the slopes at the sides of the surface. This so-called second-strike effect is also not included in our model. Further differences are the round top of the experimental holes, due to the finite particle size and the widening of the experimental holes due to mask wear.

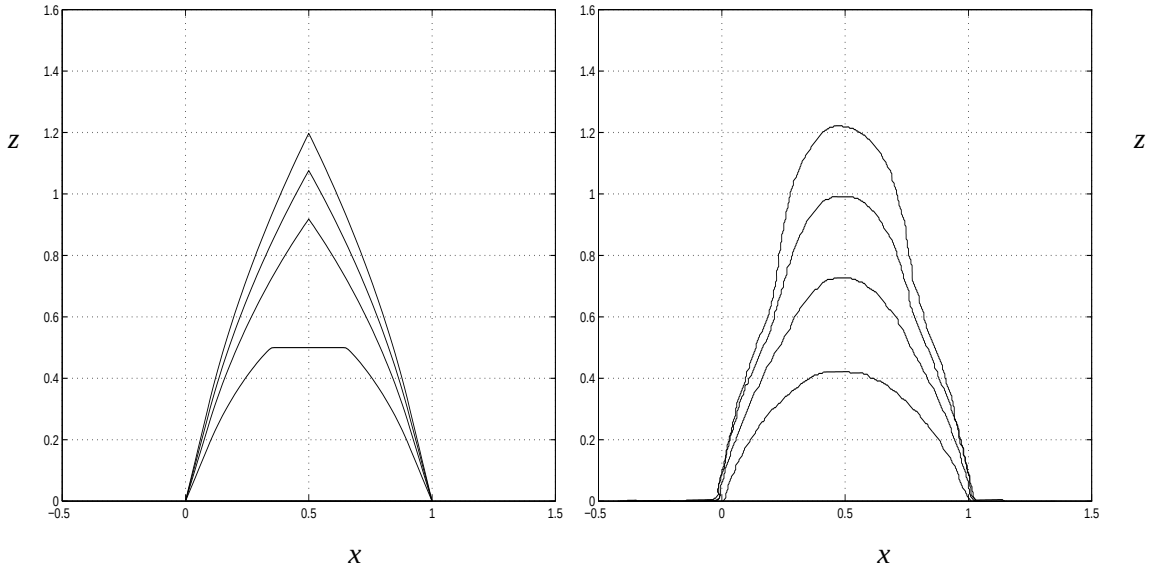

Figure 6: Analytical solution (left) and measurements (right) of the surface position for a one-dimensional trench at $t = 0.5$, 1.1, 1.6 and 2.1. (Experimental results by P.J. Slikkerveer [18])

Acknowledgements. The authors would like to thank J. Boersma for critically reading the manuscript and for the many valuable suggestions which helped to improve the text.

References

[1] Abramowitz, M. and Stegun, I.A. (Eds.): Handbook of Mathematical Functions. National Bureau of Standards, Washington (1964).

[2] Ballout, Y., Mathis, J.A. and Talia, J.E.: Solid particle erosion mechanisms in glass. Wear 196: 263-269 (1996).

[3] Buijs, M.: Erosion of glass modelled by indentation theory. J. Am. Ceram. Soc. 77: 1676-1678 (1994).

[4] Carter G. and Nobes, M.J.: The theory of development of surface morphology by sputter erosion processes. In: Aucello, O. and Kelly, R. (eds): Ion bombardment modification of surfaces: 163-224, Elsevier, Amsterdam (1984).

[5] Feng, Z. and Ball, A.: The erosion of four materials using seven erodents- towards an understanding. Wear 233-235: 674-684 (1999).

[6] Gorkom, G.G.P. van, Baller, T.S., Hendriks, B.H.W., Lambert, N., Ligthart, H.J., Montie, E.A., Thomas, G.E., Trompenaars, P.H.F. and Zwart, S.T. de: Flat thin CRT based on controlled electron transport through insulated surfaces. Appl. Surf. Sci. 111: 276-284 (1979).

[7] Hutchings, I.M.: Transitions, threshold effects and erosion maps. Key Eng. Mater. 71:75-92 (1992).

[8] Katardjiev, I.V., Carter, G., Nobes, M.J., Berg, S. and Blom, H.O.: Three dimensional simulation of surface evolution and erosion. J. Vac. Sci. Technol. A 12, vol. 1: 61-68 (1994).

[9] Kevorkian, J.: Partial differential equations, Analytical solution techniques. Wadsworth & Brooks, Pacific Grove (1990).

[10] Ligthart, H.J., Slikkerveer, P.J., in 't Veld, F.H., Swinkels, P.H.W. and Zonneveld, M.H.: Glass and glass machining in Zeus panels. Philips J. Res. 50: 475-499 (1996).

[11] Murugesh, L. and Scattergood, R.O.: Effect of erodent properties on the erosion of alumina. J. Mater. Sci. 26: 5456-5466 (1991).

[12] Sheldon, G.L.: Similarities and differences in the erosion behaviour of materials. Trans. ASME J. Basic. Eng. 92: 619-626 (1970).

[13] Slikkerveer, P.J., Bouten, P.C.P., in 't Veld, F.H. and Scholten, H.: Erosion and damage by sharp particles. Wear 217: 237-250 (1998).

[14] Slikkerveer, P.J. and in 't Veld, F.H.: Model for patterned erosion. Wear 233-235: 377-386 (1999).

[15] Slikkerveer, P.J.: Mechanical Etching of Glass by Powder Blasting. Ph.D. Thesis, Eindhoven University of Technology (1999).

[16] Sparks, A.J. and Hutchings, I.M.: Transitions in erosive wear of a glass ceramic. Wear 149: 99-110 (1991).

[17] Tannas Jr, L.E.: Flat panel displays and CRT's, Van Nostrand Reinhold, New York (1985).

[18] ten Thije Boonkkamp, J.H.M. and Slikkerveer, P.J.: Mathematical modelling of erosion by powder blasting. Accepted for publication in Surveys on Mathematics for Industry.

[19] Walker, A.J., Borchert, M.T., Vriezema, C.J. and Zalm, P.C.: Influence of surface topography on depth profiles obtained with secondary-ion mass spectroscopy. Appl. Phys. Lett. 57,no 22: 2371-2373 (1990).

[20] Wiederhorn, S.M., Lawn, B.R. and Hockey, B.J.: Effect of particle impact angle on strength degradation of glass. J. Am. Ceram. Soc. 62: 639-640 (1979).